frontiers in Earth Science

ORIGINAL RESEARCH
published: 30 November 2021
doi: 10.3389/feart.2021.786051

Geochemical Characteristics of Hydrothermal Volatiles From Southeast China and Their Implications on the Tectonic Structure Controlling Heat Convection

Jiao Tian[1,2,3], *Yiman Li*[2,3], *Xiaocheng Zhou*[1]*, *Zhonghe Pang*[2,3], *Liwu Li*[4], *Lantian Xing*[4] and *Zhongping Li*[4]

[1]Institute of Earthquake Forecasting, China Earthquake Administration, Beijing, China, [2]Institute of Geology and Geophysics, Chinese Academy of Sciences (CAS), Beijing, China, [3]Key Laboratory of Shale Gas and Geological Engineering, Institute of Geology and Geophysics (CAS), Beijing, China, [4]Key Laboratory of Petroleum Resources Research, Northwest Institute of Eco-environment and Resources, Chinese Academy of Science, Lanzhou, China

OPEN ACCESS

Edited by:
Haibing Shao,
Helmholtz Centre for Environmental Research (UFZ), Germany

Reviewed by:
Wenjing Lin,
Chinese Academy of Geological Sciences, China
Nevzat Özgür,
Süleyman Demirel University, Turkey

***Correspondence:**
Xiaocheng Zhou
zhouxiaocheng188@163.com

Specialty section:
This article was submitted to Economic Geology, a section of the journal Frontiers in Earth Science

Received: *29 September 2021*
Accepted: *01 November 2021*
Published: *30 November 2021*

Citation:
Tian J, Li Y, Zhou X, Pang Z, Li L, Xing L and Li Z (2021) Geochemical Characteristics of Hydrothermal Volatiles From Southeast China and Their Implications on the Tectonic Structure Controlling Heat Convection. Front. Earth Sci. 9:786051. doi: 10.3389/feart.2021.786051

Hot springs and igneous rocks are present widely in southeast China, influenced by the subduction of the Western Pacific and Philippine Sea Plates. This study reports on new data of chemical compositions and He–Ne–C isotopes for gas samples from representative hot springs and wells in the Guangdong and Fujian provinces to identify the origin of hydrothermal volatiles and provide insight into geothermal tectonic affinities. The primary hydrothermal volatile component from southeast China is atmospheric N2, with a volumetric percentage of 82.19%–98.29%. It indicates medium-low temperature geothermal systems where geothermal fluids suffered a shallow circulation in closed fracture systems. Low CO_2 and CH4 contents and their depleted δ13C values confirmed the small number of deep-derived components in the study area. However, spatially discernible geochemical characteristics imply enhanced hydrothermal fluid convection in the adjacent area of the two provinces, including the Fengshun, Zhangzhou, Longyan, and Sanming geothermal fields. Specifically, the He–Ne isotopes from this area exhibit mantle He contribution of more than 10% and mantle heat flow accounts for more than half of the total heat flow. Moreover, according to the thermal background calculations, the highest heat flow value of 77.7 mW/m^2 is indicated for the Zhangzhou geothermal area and the lowest value of 54.7 mW/m^2 is indicated for the Maoming geothermal area. Given the epicenter distributions and the corresponding earthquake magnitudes, the NE-trending faults are heat-control tectonic structures and their intersections with the NW-trending faults provided expedite channels for geothermal fluids rising to the surface. Therefore, the preferred development potential of geothermal resources can be expected in the adjacent area of the two provinces where two sets of active faults crossed. This study provides critical information on understanding the geothermal distribution controlled by the tectonic structure in southeast China.

Keywords: Southeast China, geothermal gas, heat-control structure, thermal background, hot springs

1 INTRODUCTION

Convective geothermal systems, also called fracture-controlled geothermal systems, are formed *via* deep-water circulation in tectonically active areas (Santilano et al., 2015). Regional tectonic structures, where extensional channels formed by crossed faults provide channels for geothermal fluid rising to the surface (Jolie et al., 2015), control the formation of this type of system. This type of geothermal system is prominent in nonvolcanic areas with high-temperature backgrounds. The depth of the faults

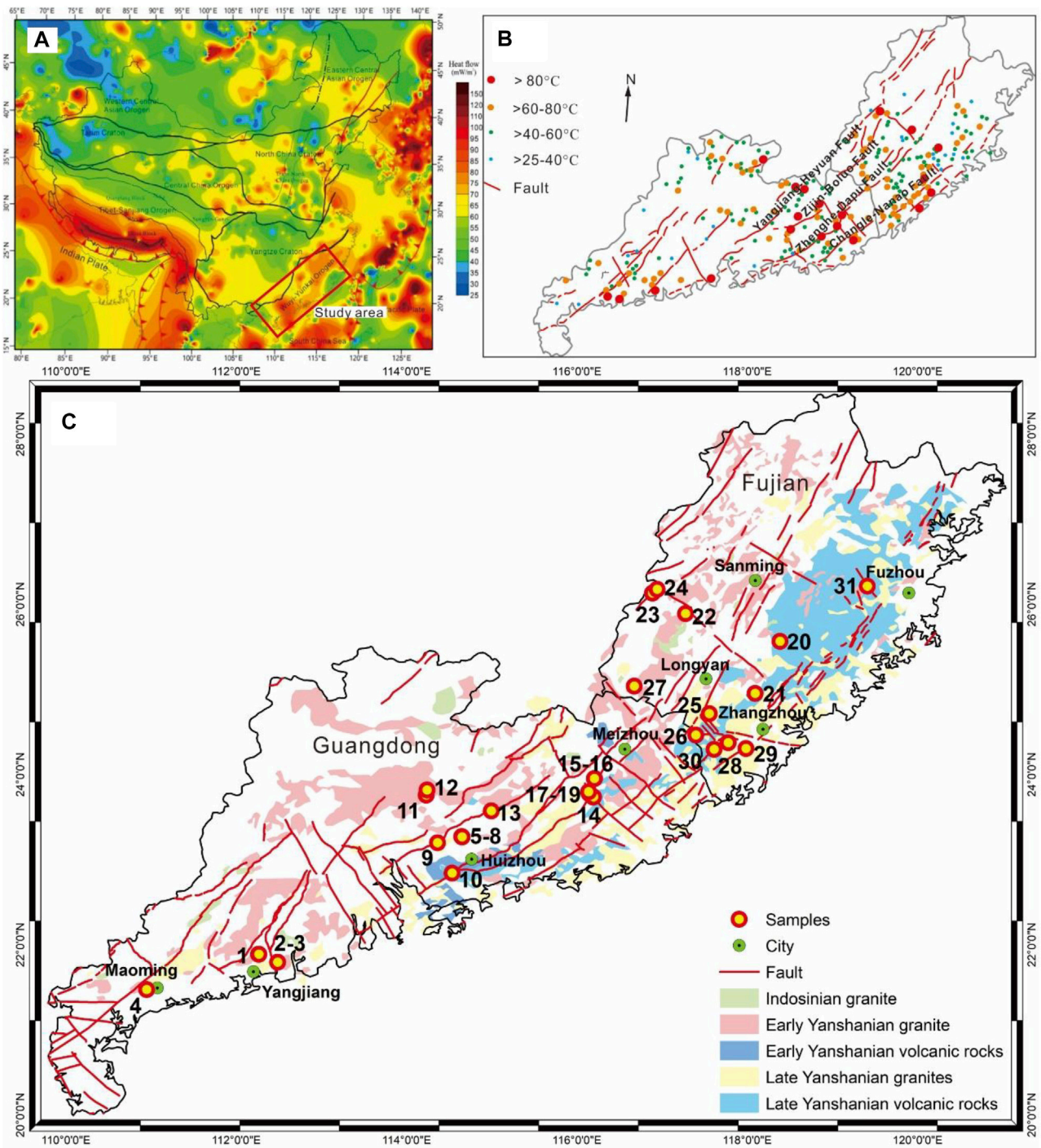

FIGURE 1 | (A) Heat flow map of continental China (Jiang et al., 2019). **(B)** Hot spring and active faults in the study area (Guangdong and Fujian provinces). **(C)** Igneous rocks (Li et al., 2012) and sampling sites in this study (the sampling points are labeled with numbers, which are consistent with those listed in the "No." column in **Table 1**. For the samples located tightly in the study area, they are labeled as a range, for example, "5–8" represents sample number range from 5 to 8).

significantly influences the reservoir temperature. For example, in the eastern edge of the Qinghai–Tibet Plateau, the Xianshuihe fault, an active lithospheric-scale strike-slip fault, functions as a conduit for deep-derived geothermal volatiles, and enhances the heat convection process down to a depth of 8 km, forming high-temperature geothermal systems with reservoir temperatures as high as 260°C. However, in the Longmenshan Thrust fault zone, the shallow groundwater circulation in relatively closed fracture systems accounts for its low reservoir temperature (<150°C), with a circulation depth of less than 4 km (Tian et al., 2021). Thus, extensional deep faults in convective geothermal systems are typically the focus of geothermal exploration as preferential targets for high-temperature geothermal resources.

Located in the coupled domain between the two global geothermal belts, southwest China is a segment of the Mediterranean–Himalayas geothermal belt and southeast China belongs to the Circum–Pacific geothermal belt. These two geothermal belts are marked with high heat flow values (**Figure 1A**). For the southwest part, the Qinghai–Tibet Plateau has attracted the attention of many researchers to conduct studies on how tectonic structures control hot spring distributions (Guo, 2012; Hochstein and Regenauer-Lieb, 1998; Liao and Zhao, 1999). Studies on hydrothermal volatiles were critical in identifying the influence of tectonic structures on geothermal exhibitions (Tian et al., 2021; Zhang et al., 2021; Zhou et al., 2017). The southeast Chinese mainland is characterized by widespread Jurassic–Cretaceous granitic magmatism (**Figures 1B,C**) associated with more than 500 hot springs exposed along a series of NE-trending faults, with temperatures of 50°C–100°C (Pei and Hong, 1995; Jiang et al., 2019). According to recent broadband magnetotelluric (MT) results, no magma chamber or partial melt exists beneath the geothermal systems, and radiogenic heat produced from decaying radioactive elements in the crust is the heat source of southeastern China (Cheng et al., 2021). Therefore, the depth of circulation controlled by active faults could be a critical factor affecting reservoir temperatures. However, only a few hydrothermal studies have focused on the flow path of geothermal water in limited or individual regions in this area (Mao et al., 2015; Qiu et al., 2018; Mao et al., 2020). Genetic models for geothermal volatile origins have not been fully integrated into the geodynamic setting, and a comprehensive understanding of the mechanism of fault controlling hot spring distributions remains deficient for southeast China.

Geothermal gas studies allow tracing deep mass and energy inputs from shallow, meteoric-dominated, and geothermal reservoirs (Lowenstern et al., 2015). Specifically, isotopic and elemental compositions of He, CO_2, and N_2 in the gases are sensitive tracers of crustal and mantle components in the overall volatile inventory (Hilton et al., 2002; Smith et al., 2005; Sano et al., 2017). Furthermore, the melting and stress-induced dilatancy of deep-seated rocks can cause detectable changes in volatile geochemistry (Zhang et al., 2021). Thus, geothermal volatiles have been used as an effective tool for understanding tectonic structures (Hoke et al., 2000; Newell et al., 2008). They provide significant information on active structures and upflow conduit distributions for geothermal fluids in a specific region. In this study, we report chemical compositions and He–Ne–C isotopes for geothermal gas samples from representative hot springs and drilled wells in the Guangdong and Fujian provinces, southeast China, to identify the origin and evolution of hydrothermal volatiles. Finally, this study provides insight into the tectonic affinities with a geothermal distribution in such granite–hosted area.

2 GEOLOGICAL SETTING

As shown in **Figure 1A**, southeast China is a high-heat flow area in the Chinese mainland. Belonging to Wuyi–Yunkai Orogen and located at the junction of the three tectonic systems of the Pacific, Paleo–Asian, and Tethys Oceans, southeast China mostly comprises the Cathaysia Block, Jiangnan Orogen, and Yangtze Block. The interaction among these energetic tectonic domains aerated widespread intracontinental deformation in South China, including intracontinental rifting, a large-scale strike-slip fault with transtension and transpression properties, and an extensional basin (Tannock et al., 2020). Pre-Neoproterozoic crystalline basement rock outcrops are scarce in South China. The Middle–Late Neoproterozoic geology of the South China Block was characterized by continental rifting and widespread anorogenic magmatism since 850 Ma (Wang and Li, 2003; Carter and Clift, 2008). The change in regional tectonic stress from Mesozoic extension to Cenozoic compression in South China is accompanied by the mid-crustal quartz-reef formation in the former to a strike-slip-associated upper-crustal hydrological fault-hosted permeability network (Tannock et al., 2020). The Cenozoic South China tectonic deformation is complex, including coupled rifting and intraplate volcanism faults, uplifting events, a large-scale termination of basin development, and volcanism. The deformation was originally considered to be because of the impact of the Pacific Plate subduction; however, an increasing number of multidisciplinary studies propose that the India–Eurasia collision has a tremendous or decisive effect on the tectonic evolution of South China and even East Asia (Yin, 2010; Gong and Chen, 2014; Wu et al., 2018; Tannock et al., 2020).

The South China Block experienced multistage tectonomagmatic events from the Proterozoic to the Late Mesozoic, contemporaneous with the Indosinian tectonic event in the Indochina Block, forming an intracontinental orogenic belt with a width of approximately 1,300 km and exposing a large area of Mesozoic igneous rocks (Li et al., 2012; Li, 2000). Early Paleozoic granites are widespread in the eastern South China Block. These rocks were mostly dated at 450–420 Ma (Li et al., 2010). Late Paleozoic igneous rocks are exposed only in 290–260 Ma potassic to calc-alkaline intrusive rocks in the Hainan Island and 250 Ma syenites in the Wuyishan Mountains. Mesozoic igneous rocks occur over a vast area in the Fujian and Guangdong provinces. Among these rocks, granites and rhyolites account for nearly 50% each, whereas gabbros and basalts are rare, and diorite and andesites are even less common (Zhou and Li, 2000). They are subdivided into the Triassic (Indosinian-aged), Jurassic (Early Yanshanian),

and Cretaceous (Late Yanshanian) (**Figure 1C**) (Zhou et al., 2006; Li et al., 2012). Indosinian magmatic rocks dominated by plutonic bodies account for only 6.6% of the Mesozoic magmatic rocks. Crustal uplift and subsidence control the Early Yanshanian granites, mostly comprising plutonic intrusive rocks. This is related to crustal thickening caused by the horizontal compression stress field. Since the late Yanshanian, many crust-mantle mixed-source alkaline granite belts and Cenozoic alkaline basalts have appeared, following crustal thinning of the lithosphere of the South China Block (Li et al., 2010; X. et al., 2000).

The multiple tectonic events are characterized by crust shortening deformation and form a tectonic framework of an interpenetrative fault system with dominant NE-trending, concomitant NW-trending and supplementary EW-trending faults. Here, the Yanshannian deformation is characterized by wide NNE-trending thrust-and-fold belts (Li et al., 2019). NNE- and NE-trending faults and NW-trending faults interweave to form a complex fault system controlling tectonic evolution, magmatic activity, geothermal activity, and mineralization. From the north to the south, lithospheric scale faults include the Yangjiang–Heyuan normal fault, the Zijin–Boluo thrust, the Zhenghe–Dapu normal, and the Changle–Nanao normal-dextral strike-slip faults (**Figure 1B**) (Tong and Tobisch, 1996; Shu et al., 2009). As recorded, the thicknesses of the continental crust and the lithosphere of East China are 30–35 and 70 km, respectively. The upwelling asthenosphere heats the thinned lithosphere, developing basin and mountain systems. Consequently, the mantle heat flow significantly increases, accompanying widespread low-medium temperature springs, Cenozoic magmatism, active faults, and earthquakes. Thus, the high heat flow (65–100 Mw m^{-2}) of southeast China corresponds to the thinning of the lithosphere (Zhao G. et al., 1998; Jiang et al., 2019).

3 SAMPLING AND METHODS

In this study, geothermal gas samples were collected from 31 sites, including natural springs and drilled wells. For the bubbling springs, a Teflon funnel that was invertedly submerged into the geothermal spring was used. For drilling wells, a copper cooling coil was connected to the sampling valve on the wellhead. By sinking the cooling coil into cold water, the geothermal fluid was cooled to a temperature lower than 20°C to enhance the degassing process. After the pipe-flushing step, the gas drainage method using a lead glass bottle connected by a silicone tube to the funnel or the cooling coil gathered gaseous samples. After the gas filled approximately two-thirds of the glass bottle volume, the bottle was sealed with a rubber cap. Subsequently, the bottle was encapsulated in a 500-ml brown polyethylene bottle filled with the *in situ* geothermal water to avoid atmospheric contamination (Tian et al., 2021). For each sampling site, three parallel samples are collected and used for determining the gas composition, $^{3}He/^{4}He$ and $^{4}He/^{20}Ne$ ratios, and $\delta^{13}C_{V\text{-}PDB}$ (CO_2 and CH_4) values, respectively. Unfortunately, two samples (HZ12 and HZ13) were destroyed during transit, and their $\delta^{13}C_{V\text{-}PDB}$ values could not be determined.

All samples were analyzed within 1 month after the fieldtrip in the Key Laboratory of Petroleum Resources in the Northwest Institute of Eco-Environment and Resources, Chinese Academy of Sciences. Gas compositions were determined using a mass spectrometer MAT 271 with relative standard deviations of less than 5%. The detection limit is 0.0001%. The $^{3}He/^{4}He$ and $^{4}He/^{20}Ne$ ratios were analyzed using a Noblesse noble gas mass spectrometer produced by Nu Instruments, United Kingdom. Air from the Gaolan Hill south of Lanzhou calibrated the instrument. The $\delta^{13}C_{V\text{-}PDB}$ (CO_2 and CH_4) values were determined using the GC-IRMS analytical system gas chromatography (Agilent 6,890) stable isotope ratio mass spectrometer (Thermo-Fisher Scientific Delta Plus XP), coupled with an online sample preprocessor (Zhou et al., 2017). The conventional delta notation per mil (‰) expressed the C isotopic ratios following the Pee Dee Belemnite (PDB) from South Carolina. The measurement errors for carbon isotopic ratios were ±0.2‰, and the analytical precision of $\delta^{13}C$ was 0.3‰.

4 RESULTS

As shown in **Table 1**, the primary component of hydrothermal volatiles from the southeastern China mainland is N_2, with a volumetric percentage range of 82.19%–98.29%. It is followed by variable amounts of CO_2, CH_4, H_2, He, O_2, Ar and other trace gases, such as CO and C_2H_6. The H_2S, SO_2, C_2H_4, and C_3H_8 contents in these samples are lower than the detection limit (0.0001%). O_2 in the gas components indicates that air contamination occurred during either the sampling or measurement.

Except for SM22 which has CO_2 (75.65 vol%) as a major component, the CO_2 content in the study area is lower (0.02%–10.27%) than typical high-temperature geothermal areas with volumetric percentages higher than 80%. For example, the CO_2 content in the Yangbajing, Tengchong, and Batang geothermal systems from the Himalayan geothermal belt is as high as 95.2% (Zhao P. et al., 1998), 86% (Zhang et al., 2016), and 98.75% (Tian et al., 2018), respectively. In the Mud Volcano from the Yellowstone geothermal system, US, CO_2 accounts for 99.5% of noncondensable gas (Lowenstern et al., 2015). CO_2 is also the main gaseous component in Icelandic geothermal areas and represents 80%–99% (Ármannsson, 2016).

The volumetric contents of H_2 and CH_4 are lower than 0.22 and 2.21%, respectively. The He content ranges between 10 and 7,098 ppmv, which is less than 1%. No abnormally high content for these constituents was shown in this area. However, these constituents could indicate specific geological conditions. For instance, high H_2 concentrations (2.4%–99%) were recognized in the Jimo geothermal system on China's eastern coast, indicating its underlying basaltic bedrock where the oxidation of Fe^{II}-rich pyroxene and olivine occurred (Hao et al., 2020). He contents as high as 2.52% were identified in Guanzhong Basin geothermal system in northwestern China, and it is attributed to the million-year circulation of groundwater and the corresponding

TABLE 1 | Chemical composition of hydrothermal volatiles from Southeast China in this study ("-" represents the content lower than the detection limit 0.0001%).

Location	No	T (°C)	Latitude (°)	Longitude (°)	He (ppm)	N_2 (%)	CO_2 (%)	CH_4 (%)	H_2 (%)	O_2 (%)	Ar (%)	CO (%)	C_2H_6 (%)
Yangjiang	YJ1	89	21.889056	112.261786	2,336	96.21	1.11	0.58	—	0.34	1.56	—	—
	YJ2	86	21.889111	112.265767	1,684	96.33	0.46	0.53	0.0260	0.92	1.54	—	—
	YJ3	80	21.795881	112.485256	2,221	94.34	0.89	0.31	0.2200	2.45	1.54	—	—
Maoming	MM4	80	21.473411	110.946908	1,771	95.44	1.82	0.15	0.0003	0.90	1.50	—	—
Huizhou	HZ5	55	23.268756	114.649539	3,714	82.19	10.27	1.58	0.1700	4.28	0.92	—	—
	HZ6	52	23.270883	114.647947	3,081	83.89	9.12	1.14	0.1300	4.26	0.99	—	0.0015
	HZ7	50	23.270633	114.648361	1,313	94.13	0.89	0.64	0.0002	3.10	1.06	—	—
	HZ8	50	23.268542	114.650747	5,587	90.46	7.13	0.32	0.0003	0.24	1.02	0.0017	—
	HZ9	56	23.200103	114.363697	3,716	95.8	0.44	1.23	0.0005	0.90	1.16	0.0052	—
	HZ10	41	22.841883	114.534281	10	95.23	0.042	2.21	0.0003	1.24	1.27	—	—
	HZ11	54	23.759094	114.231308	2,486	95.36	1.24	0.29	0.0005	1.61	1.19	—	—
	HZ12	54	23.820247	114.239425	702	91.04	0.1	0.10	0.0330	7.50	1.16	0.0110	—
	HZ13	42	23.573350	114.994322	178	98.29	0.22	0.01	0.0001	0.38	1.09	—	—
Fengshun	FS14	89	23.736031	116.192108	967	91.37	3.97	0.32	0.0350	2.67	1.56	—	—
	FS15	96	23.953317	116.206367	1,816	95.68	0.2	0.37	0.1400	1.99	1.48	—	—
	FS16	82	23.954178	116.205147	2,501	95.97	0.83	1.03	0.0008	0.31	1.60	—	—
	FS17	94	23.775528	116.144239	1,184	90.28	0.36	0.17	0.0025	7.70	1.39	—	—
	FS18	54	23.737144	116.194658	617	96.51	0.28	0.78	0.0001	1.11	1.26	—	—
	FS19	60	23.797300	116.137594	759	89.11	0.11	0.24	0.0270	9.34	1.09	—	—
Zhangzhou	ZZ20	90	25.567022	118.384899	3,761	94.27	1.20	1.59	0.0040	0.54	1.77	—	—
	ZZ21	82	24.953542	118.091856	2,512	94.32	0.02	0.04	0.0063	1.97	1.28	—	—
	ZZ25	58	24.716668	117.554358	1,433	96.32	0.37	0.06	0.0001	1.45	1.32	—	—
	ZZ26	75	24.463856	117.395976	2,826	96.71	0.92	0.08	0.0028	0.42	1.35	—	—
	ZZ28	66	24.374366	117.777054	1,274	96.67	1.79	0.18	0.0005	0.30	1.39	—	—
	ZZ29	65	24.307501	117.984466	1,249	95.06	0.23	0.06	0.0151	0.77	1.13	—	—
	ZZ30	70	24.297266	117.611400	1,523	97.28	0.15	0.03	0.0012	0.64	1.44	—	—
Sanming	SM22	72	25.892461	117.274494	484	19.22	75.65	0.04	0.0001	1.69	0.21	—	—
	SM23	54	26.130642	116.886600	7,098	92.59	4.90	0.34	0.0001	0.52	1.22	—	—
	SM24	76	26.176875	116.941361	6,863	92.29	3.41	0.74	0.0006	0.65	1.42	—	—
Longyan	LY27	68	25.040260	116.673924	4,599	94.30	2.28	0.04	0.0001	1.14	1.14	—	—
Fuzhou	FZ31	81	26.214173	119.410192	2,491	95.77	0.13	0.08	0.0018	0.53	1.72	—	—

accumulation of gaseous components in the reservoir (Li et al., 2017). Furthermore, the high CH_4 content (up to 60.95%) in the Niutuozhen geothermal field, North China, indicates organic sediments existing in the reservoir rocks (Pang et al., 2018). Therefore, low H_2, CH_4, and He concentrations indicate that the abovementioned geologic conditions could not occur in the study area.

As shown in **Table 2**, the measured $^3He/^4He$ ratios of samples range from 1.07×10^{-7} to 1.95×10^{-6}, 0.08 Ra–1.39 Ra (where Ra denotes the atmospheric $^3He/^4He = 1.39 \times 10^{-6}$). The $^4H/^{20}Ne$ ratio is 2.8–646. Because ^{20}Ne is assumed to originate from the atmosphere (Craig et al., 1978), $^4H/^{20}Ne$ ratios are used to evaluate air contamination levels in samples. All $^4H/^{20}Ne$ ratios are more than two orders of magnitude larger than the atmospheric value of 0.318 (Sano and Wakita, 1985), indicating that minimum atmospheric contamination occurred during sampling and He/Ne isotope measurements. As summarized in **Table 2**, the measured $^3He/^4He$ ratios were corrected (R_c) for air contamination using the method proposed by Craig (1978), and only slight differences occurred for samples with relatively lower $^4H/^{20}Ne$ ratios, such as HZ10, HZ12, and HZ13.

As reported in **Table 2**, the $\delta^{13}C$ values (versus PBD) for CO_2 and CH_4 of the samples ranged from −19.6‰ to −6.7‰ and from −65.4‰ to −8.8‰, respectively. These carbonic isotopic ratios exhibit values lower than those from the high-temperature geothermal systems in the Chinese mainland. In the Batang geothermal system, the eastern edge of the Qinghai-Tibet Plateau, the $\delta^{13}C$ contents of CO_2 and CH_4 were −7.7‰ to −0.5‰ and −40.2‰ to −21.1‰, respectively (Tian et al., 2018). In the Yangbajing geothermal system, $\delta^{13}C_{CO2}$ values were −11.3‰ and −7.7‰ (Zhao P. et al., 1998). In Tengchong volcanic geothermal area, the range of $\delta^{13}C$ values for CO_2 and CH_4 are −9.0‰ to −2.1‰ and −25.5‰ to −9.7‰, respectively (Zhao et al., 2011; Zhang et al., 2016). This comparison shows that the evolution process of hydrothermal volatiles from the southeast China is different from the abovementioned areas and the probability of feeding high-temperature geothermal reservoirs in such geological settings remains to be studied.

5 DISCUSSION

5.1 Origin of Essential Gaseous Components

5.1.1 Nitrogen and Argon

As mentioned in the **Section 4**, CO_2, a prominent component of mantle volatiles, is the major component in high-temperature geothermal systems in magmatic areas (Lowenstern et al., 2015; Ármannsson, 2016). However, N_2 domination is a typical characteristic for medium-low temperature geothermal

TABLE 2 | Isotopic composition of hydrothermal volatiles in this study area ("n.a." represents no analysis).

No	$\delta^{13}C_{CH4}$ (‰)	$\delta^{13}C_{CO2}$ (‰)	$^{4}He/^{20}Ne$	R	R/Ra	Rc	Rc/Ra	q (mW/m^2)	qc (mW/m^2)	qm (mW/m^2)	T–40 km (°C)	T–50 km (°C)
YJ1	−45.4	−17.5	131	5.00E−07	0.36	4.98E−07	0.36	67	35	32	821	935
YJ2	−47.1	−17.1	91	6.53E−07	0.47	6.51E−07	0.47	69	35	34	855	975
YJ3	−45.3	−16.9	132	6.12E−07	0.44	6.10E−07	0.44	69	35	33	848	966
MM4	−40.9	−14.5	109	1.11E−07	0.08	1.07E−07	0.08	55	34	21	631	715
HZ5	−46.5	−11.4	492	7.09E−07	0.51	7.08E−07	0.51	70	35	35	867	988
HZ6	−56.8	−13.4	265	6.95E−07	0.50	6.94E−07	0.50	70	35	34	863	984
HZ7	−61.9	−17.0	70	7.51E−07	0.54	7.48E−07	0.54	70	35	35	873	995
HZ8	−51.3	−14.6	646	6.67E−07	0.48	6.67E−07	0.48	69	35	34	859	979
HZ9	−62.0	−16.3	303	5.84E−07	0.42	5.83E−07	0.42	68	35	33	842	959
HZ10	−50.2	−19.6	3	6.26E−07	0.45	5.28E−07	0.38	69	36	33	850	968
HZ11	−48.8	−16.5	166	4.17E−07	0.30	4.15E−07	0.30	65	35	30	798	909
HZ12	n.a	n.a	33	2.22E−07	0.16	2.11E−07	0.15	61	35	25	723	822
HZ13	n.a	n.a	7	5.14E−07	0.37	4.74E−07	0.34	67	36	31	825	939
FS14	−62.1	−15.6	53	1.35E−06	0.97	1.35E−06	0.97	75	34	41	946	1,079
FS15	−58.0	−16.7	78	1.04E−06	0.75	1.04E−06	0.75	73	35	38	914	1,042
FS16	−58.4	−15.8	182	1.32E−06	0.95	1.32E−06	0.95	75	34	41	943	1,076
FS17	−55.6	−17.1	57	6.39E−07	0.46	6.35E−07	0.46	69	35	34	855	974
FS18	−34.6	−19.4	31	8.62E−07	0.62	8.56E−07	0.62	71	35	36	889	1,014
FS19	−54.9	−16.6	43	1.11E−06	0.80	1.11E−06	0.80	73	34	39	923	1,053
ZZ20	−65.4	−11.1	211	4.03E−07	0.29	4.02E−07	0.29	65	35	30	797	907
ZZ21	n.a	−8.3	96	2.92E−07	0.21	2.88E−07	0.21	63	35	28	759	863
ZZ25	−8.8	−7.4	69	5.98E−07	0.43	5.94E−07	0.43	68	35	33	845	963
ZZ26	−44.5	−15.9	130	1.40E−06	1.01	1.40E−06	1.01	75	34	42	951	1,086
ZZ28	−58.2	−18.8	61	4.03E−07	0.29	3.98E−07	0.29	65	36	30	798	908
ZZ29	n.a	−16.9	51	8.20E−07	0.59	8.17E−07	0.59	71	35	36	884	1,007
ZZ30	n.a	−15.4	73	1.93E−06	1.39	1.93E−06	1.39	78	32	45	990	1,131
SM22	−57.6	−6.7	162	1.78E−06	1.28	1.78E−06	1.28	77	33	44	980	1,119
SM23	−49.1	−12.1	408	5.70E−07	0.41	5.69E−07	0.41	68	35	33	840	956
SM24	−52.2	−13.7	386	4.45E−07	0.32	4.44E−07	0.32	66	35	31	807	919
LY27	−13.2	n.a	265	1.53E−06	1.10	1.53E−06	1.10	76	33	42	961	1,097
FZ31	−19.1	n.a	109	4.87E−07	0.35	4.84E−07	0.35	67	35	31	820	933

systems, indicating that the geothermal fluid suffered a relatively shallow circulation depth through limited contact with deep-derived volatiles (Tian et al., 2021). The N_2 accumulation is due to the inert activity of nitrogen, whereas during the long-term interaction between air-saturated water and wall rocks in the reduced runoff, the oxidizing components (such as O_2) were consumed. In the comparison of the Ar/He and N_2/CO_2 ratios (**Figure 2**), the volatiles from the study area exhibit a mixing relationship between atmospheric and the geological endmembers (mantle or crustal). The shift toward high N_2/CO_2 ratios indicates the accumulation process of N_2 during the circulation path which has limited supplementary CO_2. For example, the point for ZZ21 exhibits the strongest shift of N_2 accumulation, indicating that the geothermal fluid in this area underwent long-term circulation in a relatively closed shallow fracture system. However, SM22 exhibits an opposite shift, indicating that an additional CO_2 source exists in this geothermal field. Samples from the Huizhou, Sanming, Longyan, and Zhangzhou geothermal areas exhibit more geologically derived contributions than others, indicating that either deep faults or a specific lithology affect the supplementary sources. However, it is challenging to further identify which of the two possibilities is the main factor because the excessive He could come from either the radiogenic process in the crust or the mantle volatile. Simultaneously, the metamorphic process of crustal materials and mantle–derived volatile could contribute to the CO_2. Their origins remain to be determined based on the isotopic analysis in the following sections. For the triangle plot of N_2-He-Ar in **Figure 3**, the mixing process is depicted. Since N_2 and Ar are chemically inert or only minimally reactive and have limited sources in geological environments, they are inferred to be of largely atmospheric origin in southeast China in this study. However, many samples are close to the mixing line between the endmembers of the mantle/crust and air rather than the line between the mantle/crust and air-saturated water, indicating that air contaminants affect the N_2/Ar ratios. This phenomenon is consistent with that shown by O_2. Combined with the He/Ne isotopic ratios, this air contamination is due to the measurement process of the gas composition rather than the sampling procedure because they have the same sampling method.

5.1.2 Helium

He is a critical geothermal volatile providing information on the geological setting and the regional thermal background (Polyak et al., 2000; Gautheron and Moreira, 2002). ^{3}He mainly escapes from the mantle. The predominant source is primordial He that has been trapped within the Earth from the time of its formation, whereas the reaction of ^{6}Li (n, α) ^{3}H ($^{-1}$ β) ^{3}He accounts for a negligible portion. Typically, the upper mantle sampled by the mid-ocean ridge basalts (MORB) with an R/Ra ratio of eight is

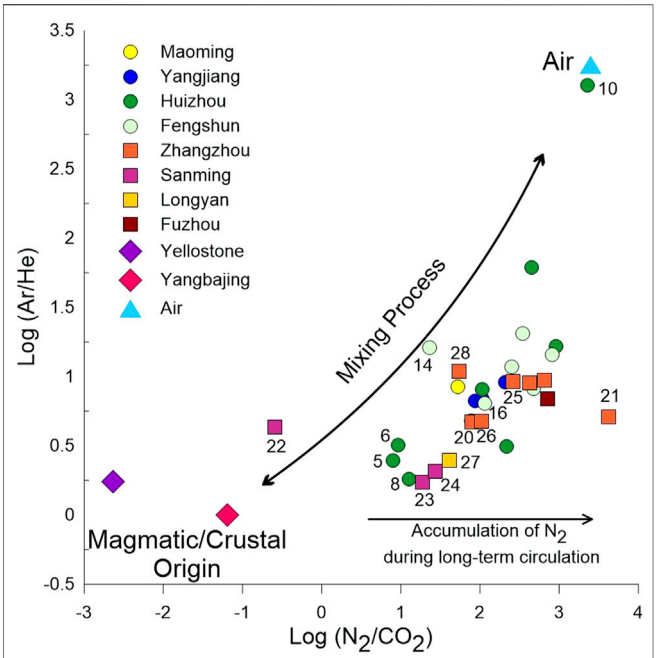

FIGURE 2 | Plot of results from gas collected from Southeast China with Log(N_2/CO_2) vs. Log(Ar/He). Samples from the Yellowstone geothermal system in the US and Yangbajing geothermal system in China represent magmatic-and crustal-derived geothermal gaseous compositions, respectively (Zhao et al., 2002; Lowenstern et al., 2015). Samples from Guangdong Province are represented by circle symbols, and those from Fujian Province are represented by rectangle symbols.

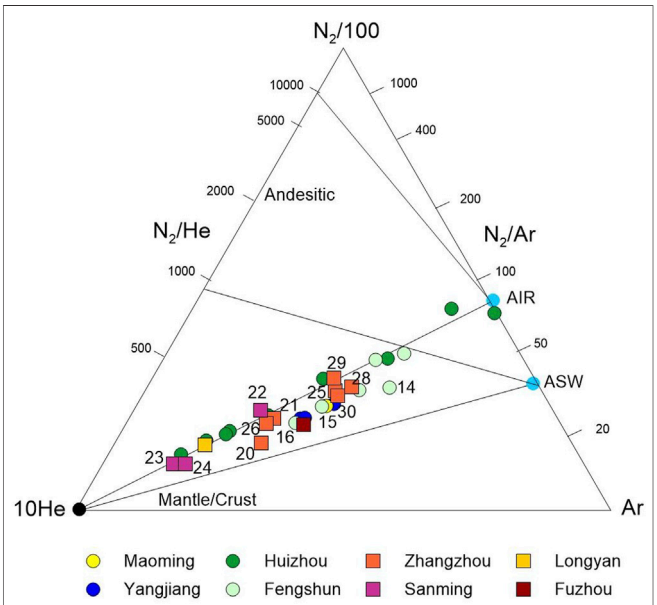

FIGURE 3 | Triangle plot of N_2-He-Ar for hydrothermal volatiles from Southeast China. The AIR represents the atmospheric component, and the ASW represents air-saturated water.

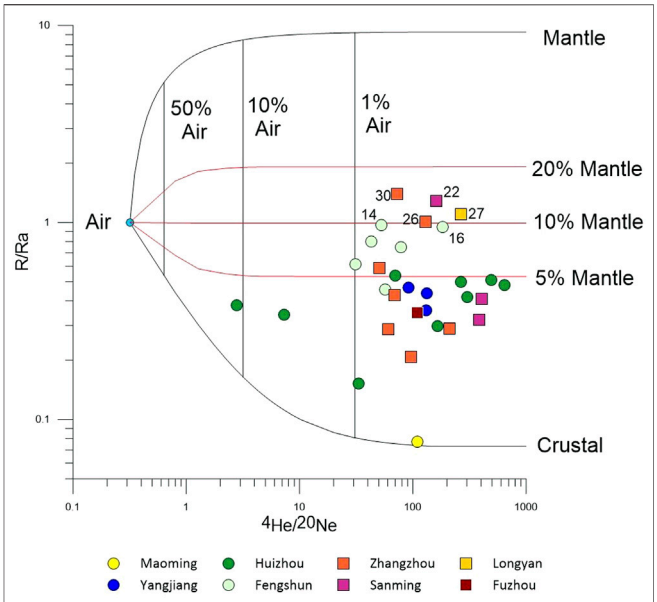

FIGURE 4 | $^4He/^{20}Ne$ ratios versus $^3He/^4He$ ratios. The $^3He/^4He$ ratios are expressed as R/Ra where R is the corrected measured ratio.

recognized as the typical asthenosphere endmember (Gautheron and Moreira, 2002). Decaying crustal U and Th predominantly produce ^4He (O'nions and Oxburgh, 1988). The conventional $^3He/^4He$ ratio of the continental crust is 0.02 Ra with a range of 0.01 Ra to 0.1 Ra (Lupton, 1983). In a specific area, the location-dependent variation of $^3He/^4He$ ratios can indicate the depth variation of fault extensions. According to the method proposed by Sano and Wakita (1985), mantle He proportions can be recognized when taking $^3He/^4He$ ratios of eight Ra and 0.02 Ra for the mantle and crustal He, respectively. From **Figure 4**, the typical crustal He isotopic ratio (0.08 Ra) is shown for the sample from the Maoming geothermal field in the south of the study area. For most of the other samples, the mantle He proportions are lower than 5%. This phenomenon indicates that radiogenic products in crustal materials mostly account for the He component. In other words, the deep-seated endmember for the geothermal volatile in the Yangjiang, Maoming, and Huizhou geothermal areas is largely crustal metamorphic rather than mantle-derived volatile. However, FS14, FS16, SM22, ZZ26, LY27, and ZZ30 exhibit mantle He contributions exceeding 10%. Because these samples are from North Guangdong and South Fujian provinces, it indicates that relative deep fault extensions and fluent uprising channels occurred in these areas. Furthermore, enhanced convection of geothermal fluids could be expected in the adjacent area of the two provinces. As illustrated in the **Section 2**, a series of NE-trending lithospheric faults in southeast China dominantly control the magmatic and geothermal activity, acting as a heat controller. However, the temperatures, chemical compositions, and isotopic compositions of geothermal volatiles exhibit distinct characteristics. According to the He isotopic ratios, a conclusion could be drawn that the NW-trending faults considerably influence constructing regional extensional conduits for fluid

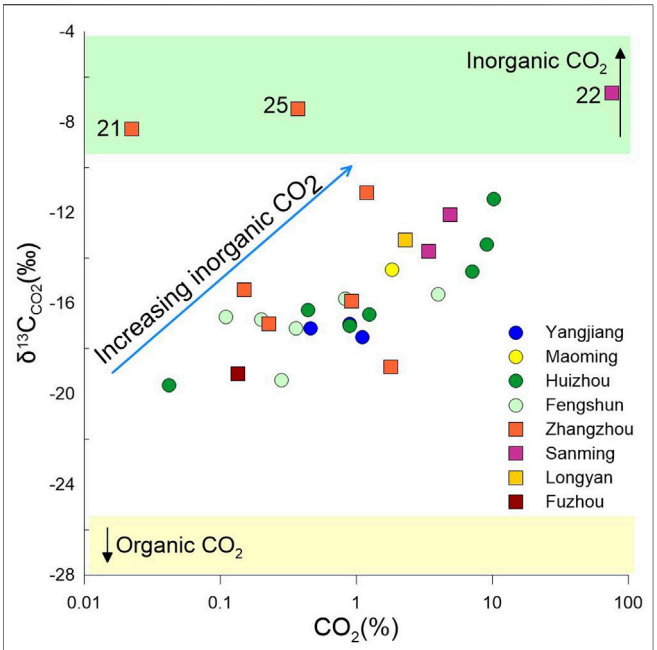

FIGURE 5 | $\delta^{13}C$ (‰) versus CO_2 for hydrothermal volatiles from Southeast China.

and heat conventions. Furthermore, **Figure 4** confirmed that air contamination during sampling is less than 1% except for two samples contaminated by 1–10%.

5.1.3 Carbon Dioxide

Biotic CO_2 is typically marked by low $\delta^{13}C$ values from −70 to −25‰ (Faure et al., 1965). Abiotic CO_2 contains a large number of heavy carbon isotopes, for example, the $\delta^{13}C$ value of carbonate metamorphic CO_2 is close to 0‰ (Sano and Marty, 1995). For the mantle-derived CO_2, the MORB ratio (−8 to −5‰) represents its isotopic ratio (Javoy et al., 1986). As shown in **Figure 5**, the CO_2 content increase is accompanied by ^{13}C isotope enrichment. For example, SM22 has the highest CO_2 content, with a volumetric percentage as high as 75.65% and a $\delta^{13}C_{CO2}$ value of −6.7‰. This CO_2-rich sample with a high $\delta^{13}C_{CO2}$ value could result from the involvement of carbonate rocks ($\delta^{13}C$). By combining its inorganic carbon composition with the He and Ne isotopic signature, a deep developed fracture system could be expected in this area. Therefore, the deep-derived volatile functions as the additional CO_2 source for the SM22. Considering the above discussion that mantle-derived volatile accounted for more than 10% in SM22, the mantle CO_2 contributes to a larger ratio in this area than those of other sampling sites. Nevertheless, the major source of inorganic CO_2 could still be attributed to carbonate metamorphic processes deep within the crust rather than mantle volatiles. Although enriched carbonic isotopes also occurred at ZZ21 and ZZ25 in the Zhangzhou geothermal area, the low CO_2 contents and low $^3He/^4He$ ratios of these sampling sites indicate that the fractures in these areas could not provide sufficiently deep volatiles. Carbonate metamorphism in the shallow crust could be the major source of geothermal volatiles. For other samples, the depleted $\delta^{13}C_{CO2}$ values can be attributed to either the organic metamorphic or degassing processes in the geothermal fluid. In the first case, hydrothermal volatiles have pervasively received contributions from inorganic and organic carbon endmembers with different mixing ratios. In the second case, the strong isotopic fractionation during the degassing process of the dissolved CO_2 results in ^{13}C depletion in the gaseous component, which occurred in areas with carbonate formations, such as the Huizhou geothermal field (Yan et al., 2019). Although it is challenging to identify the controlling mechanism, both these cases indicate trace amount of mantle CO_2 in the closed fracture systems.

5.1.4 Methane Component

Irrespective of the sample locations and CH_4 contents (**Figure 6A**), most hydrothermal CH_4 contents from southeast China exhibit depleted carbon isotopic compositions, with $\delta^{13}C_{CH4}$ values lower than −30‰. As recorded, the typical ranges for thermogenic and microbial CH_4 are −30‰ to −50‰ and −50‰ to −120‰, respectively, whereas the $\delta^{13}C_{CH4}$ values higher than −30‰ indicate abiogenic CH_4 or microbial consumption residue (Etiope and Schoell, 2014; Wilson et al., 2014; Sano et al., 2017). According to these threshold values, CH_4 from the study area is largely biogenic in the shallow crust or near the surface rather than the magmatic volatile. Furthermore, no coordinated variation occurs between $\delta^{13}C_{CH4}$ and $\delta^{13}C_{CO2}$ (**Figure 6B**), indicating that the CH_4 is not sourced from CO_2 by stoichiometrically inorganic reactions, and the carbon isotopic exchange equilibrium has not been achieved before surface exposure. This phenomenon could be linked to the lack of an underlying magma chamber or deep-extended fault where high-affinity binding exists between CH_4 and CO_2. Notably, ZZ25 ($\delta^{13}C_{CH4}$ = −8.8‰) exhibits heavy carbon isotopic compositions in both CH_4 and CO_2, whereas its He isotopic ratio is lower than 1 Ra. It could be attributed to some inorganic contribution from the specific lithology.

5.2 Heat Flow and Lithospheric Thermal Structure

The terrestrial heat flow (q, mW/m^2) indicates the magnitude of conductive heat transfer and has been commonly measured where conductive heat transfer dominates. It expresses an integral energetic effect of all processes occurring at depths (Polyak et al., 2000). For estimating the heat flow in areas with hot springs, convective heat transfer must be considered because the hydrothermal system provides a heat transfer mechanism in the crust based on geothermal fluid transport (Umeda et al., 2006; Tang et al., 2017). In continental areas, three nuclides (^{232}Th and $^{235,\ 238}U$) are the principal sources of radiogenic heat in the Earth, yielding ^4He as decay products. Furthermore, ^3He produced by the radiogenic process accounts for a negligible portion of the ^3He escaping from the mantle. Therefore, ^3He flux is in proportion to mantle heat flux, whereas the ^4He flux is linear with crustal heat flux. The rough estimation of crustal and mantle heat flow according to He isotopic ratios is given by (O'nions and Oxburgh, 1983, 1988; Polyak et al., 1979):

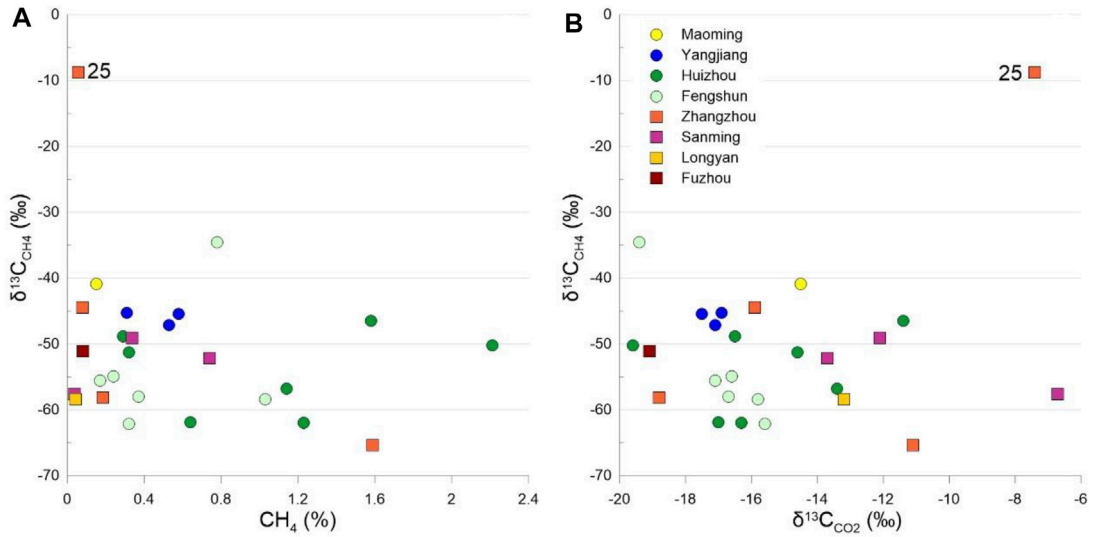

FIGURE 6 | (A) $\delta^{13}C_{CH4}$ value versus CH_4 content. **(B)** $\delta^{13}C_{CH4}$ value versus $\delta^{13}C_{CO2}$ value for hydrothermal volatiles from southeast China.

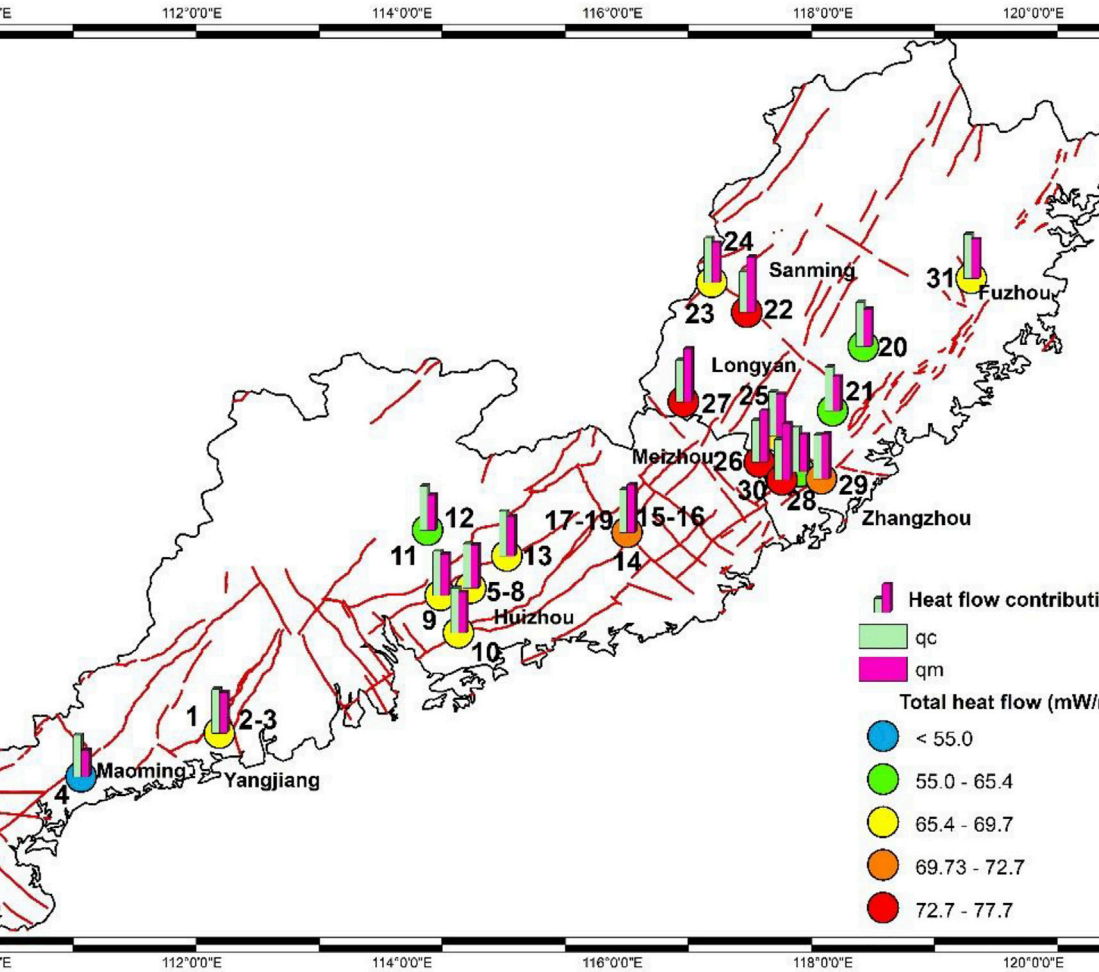

FIGURE 7 | Calculated heat flow and its contribution of crust and mantle according to He isotopic ratios of hydrothermal volatile.

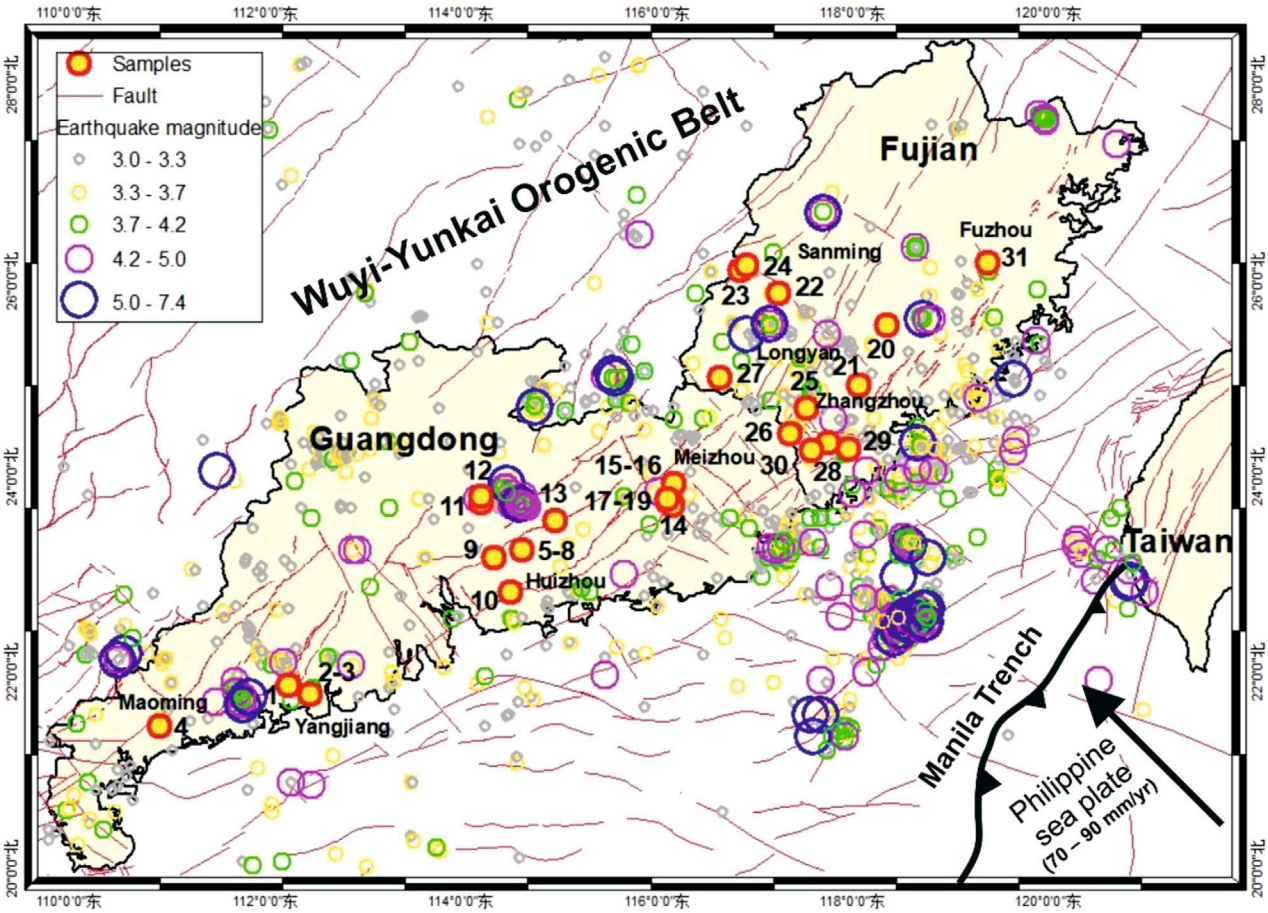

FIGURE 8 | Epicenters of Ml >3.0 earthquakes recorded during 1972–2021. Data of earthquake are from the China Earthquake Networks Center (CENC) (Ai et al., 2019).

$$q = 18.231 \log R_c + 181.82 \quad (1)$$

$$\frac{q_c}{q_m} = 0.815 - 0.3 Ln\, R \quad (2)$$

where R_c is the corrected He isotopic ratios, qc (mW/m^2) is the crustal heat flow, and qm (mW/m^2) is the mantle heat flow. Furthermore, the He isotopic data were also used to estimate the ratio between the crust and mantle heat flow components (Wang, 1999) according to **Eq. 2**. At specific depths, the heat flow q and calculated temperature T (°C) are linearly dependent with a correlation coefficient of 0.9 and higher. For depths of 40 km (the bottom of the Earth's crust) and 50 km, these dependencies are as follows (Duchkov et al., 2010):

$$T_{40} = 15.61q - 223\,(accuracy \sim \pm 40°C) \quad (3)$$

$$T_{50} = 18.09q - 275\,(accuracy \sim \pm 50°C) \quad (4)$$

These equations were used to calculate the thermal background of the study area. As shown in **Table 2**, most heat flow values are higher than the average heat flow value of continental China (63 mW/m^2) (Hu et al., 2000) and equal to the average heat flow value of South China (69.4 ± 11.0 mW/m^2) (Jiang et al., 2019). In the Zhangzhou geothermal area, the highest heat flow of 77.7 mW/m^2 (ZZ30) is indicated; however, in the Maoming geothermal area, the lowest heat flow is 54.7 mW/m^2 (MM4). The results correlate well with the heat flow values previously reported for the adjacent areas (**Figure 1A**) (Hu et al., 2000; Jiang et al., 2019). To present the heat flow distribution in **Figure 7**, we calculated the average values of hot springs crowed together, such as the average values of the following five groups: 1) YJ1, YJ2, and YJ3; 2) HZ5, HZ6, HZ7, and HZ8; 3) HZ11 and HZ12; 4) FS14, FS15, FS16, FS17, FS18, and FS19; and 5) SM23 and SM24. Notably, calculated heat flows exhibit high values in the Zhangzhou, Longyan, and Sanming geothermal areas, which are adjacent area to the two provinces and are characterized by crossed faults of the NE and NW groups. In these areas, mantle heat flow accounts for more than half of the total heat flow. Moreover, the high heat flow values are accompanied by high temperatures deep within the Earth (>900°C at 40 km and >1,000°C at 50 km). This is consistent with the above conclusion that the crossed faults function as conduits for deep-derived geothermal volatiles, but also enhance

the heat convection within the Earth. Therefore, hydrothermal systems near the boundary of the two provinces should have the highest potential for geothermal exploitation. Additionally, heat flow values for the Fengshun and Huizhou (69.0 –74.9 and 60.6–70.2 mW/m^2, respectively) also indicate their geothermal potential. Although the accuracy of these estimations remains to be further studied, the results could provide useful information about the regional variation of the lithospheric thermal structure.

5.3 Heat–Control Structure and Up–Flow Conduit

Active faults formed in the Neotectonic movement provide preferential channels for heat and mass convection in high-temperature geothermal backgrounds. To identify the activities of faults in the study area, epicenters of Ml >3.0 earthquakes that occurred from January 1972 to September 2021 were compiled in **Figure 8**. Two prominent phenomena are worth examining. On the one hand, to the southeast of the study area, the Taiwan province and its surrounding areas are earthquake–prone, where earthquakes with magnitudes higher than Ml 4.2 are concentrated. These tectonic movements are triggered by the northward subduction of the Philippine Sea Plate to the Eurasia Plate (Ai et al., 2019). Consequently, the adjacent area of the two provinces is influenced by the tectonic movements, which is proven by the high density of earthquake occurrences near Meizhou, Zhangzhou, Longyan, and Sanming. Therefore, fault activity is a controlling factor of high mantle-derived hydrothermal volatile contributions in these areas. However, the depth and permeability of faults are also significant factors for hydrothermal system formation. **Figure 8** shows the epicenters of earthquakes, especially those with high magnitudes, distributed along the NE direction. This phenomenon indicates that major tectonic movements in this area are expressed by NE-trending faults. These faults extend deeply toward the crust, where strong earthquakes originate. Simultaneously, the NE faults can provide convection conduits for heat and mass from deep within the Earth. In other words, the NE-trending faults are recognized as heat-control structures in the study area. However, the permeability of the NE faults varies. Specifically, the intersection with active NW-trending faults enhances the amount of geothermal fluid rising to the surface as verified by the discussion in the **Section 5.2**. Thus, the NW-trending faults profoundly affect the formation of upflow conduits for geothermal fluids.

6 CONCLUSION

In granite-hosted southeast China, the active faults formed during the Neotectonic movement constrain the convection of mass and heat in geothermal fluids. Based on the chemical compositions and He-Ne-C isotopes of hydrothermal volatiles, the thermal controlling structures are identified. In the geothermal volatiles, the CO_2 and CH_4 contents are low and the corresponding carbon isotopic compositions are depleted. N_2 dominates volatiles, indicating medium–low temperature geothermal systems with limited contact with deep-derived CO_2, CH_4, etc. Most He isotopic ratios exhibit typical crustal metamorphic properties; however, samples from the Longyan, Sanming, Zhanghzou, and Fengshun geothermal fields have more than 10% of mantle contribution. As calculated, the mantle heat flow accounts for more than half of the total heat flow in these geothermal fields, which is accompanied by high deep-level temperatures (>900°C at 40 km and >1,000°C at 50 km). Considering the fault system formed by the northward subduction of the Philippine Sea Plate and the eastward subduction of the Pacific Plate, it could be deduced that the deep-extended faults enhanced geothermal fluid convection in the adjacent area of the two provinces. Additionally, spatially discernible geochemical characteristics of the hydrothermal volatiles have close affinities with earthquakes that occurred in the study area. This study demonstrates that although the NE-trending faults are heat-controlling structures, the heterogeneity of geothermal volatiles is largely affected by the intersections with NW-trending faults, which provided regional expedite channels for geothermal fluid rising to the surface. Deep circulated hydrothermal systems in southeast China could be expected in the adjacent of the Guangdong and Fujian provinces.

DATA AVAILABILITY STATEMENT

The original contributions presented in the study are included in the article/supplementary material. Further inquiries can be directed to the corresponding author.

AUTHOR CONTRIBUTIONS

JT is the first author. XZ is the corresponding author. The other coauthors contributed to the sampling, determination, and analysis.

FUNDING

The study has been financially supported by the National Key R&D Program of China (Nos. 2019YFC0604901) and by the National Natural Science Foundation of China (Grant No. 41902252, 41673106, 42073063, 4193000170) and The Special Fund of the Institute of Earthquake Forecasting, China Earthquake Administration (2018IEF010104, 2019CSES0104, 2020IEF0604, 2020IEF0703, 2021IEF0602, 2021IEF0101).

REFERENCES

Ai, S., Zheng, Y., and Xiong, C. (2019). Ambient Noise Tomography across the Taiwan Strait, Taiwan Island, and Southwestern Ryukyu Arc: Implications for Subsurface Slab Interactions. *Tectonics* 38 (2), 579–594. doi:10.1029/2018TC005355

Ármannsson, H. (2016). The Fluid Geochemistry of Icelandic High Temperature Geothermal Areas. *Appl. Geochem.* 66, 14–64. doi:10.1016/j.apgeochem.2015.10.008

Carter, A., and Clift, P. D. (2008). Was the Indosinian Orogeny a Triassic Mountain Building or a Thermotectonic Reactivation Event. *Comptes Rendus Geosci.* 340 (2–3), 83–93. doi:10.1016/j.crte.2007.08.011

Cheng, Y., Han, B., Li, Y., Guo, J., and Hu, X. (2021). Lithospheric Electrical Structure beneath the Cathaysia Block in South China and its Tectonic Implications. *Tectonophysics* 814, 228981. doi:10.1016/j.tecto.2021.228981

Craig, H., Lupton, J. E., Welhan, J. A., and Poreda, R. (1978). Helium Isotope Ratios in Yellowstone and Lassen Park Volcanic Gases. *Geophys. Res. Lett.* 5 (11), 897–900. doi:10.1029/GL005i011p00897

Duchkov, A. D., Rychkova, K. M., Lebedev, V. I., Kamenskii, I. L., and Sokolova, L. S. (2010). Estimation of Heat Flow in Tuva from Data on Helium Isotopes in thermal mineral Springs. *Russ. Geol. Geophys.* 51 (2), 209–219. doi:10.1016/j.rgg.2009.12.023

Etiope, G., and Schoell, M. (2014). Abiotic Gas: Atypical, but Not Rare. *Elements* 10 (4), 291–296. doi:10.2113/gselements.10.4.291

Faure, G., Hurley, P. M., and Powell, J. L. (1965). The Isotopic Composition of Strontium in Surface Water from the North Atlantic Ocean. *Geochim. Cosmochim. Acta* 29 (4), 209–220. doi:10.1016/0016–7037(65)90018–9

Gautheron, C., and Moreira, M. (2002). Helium Signature of the Subcontinental Lithospheric Mantle. *Earth Planet. Sci. Lett.* 199 (1–2), 39–47. doi:10.1016/s0012-821x(02)00563-0

Gong, J., and John Chen, Y. (2014). Evidence of Lateral Asthenosphere Flow beneath the South China Craton Driven by Both Pacific Plate Subduction and the India-Eurasia continental Collision. *Terra Nova* 26 (1), 55–63. doi:10.1111/ter.12069

Guo, Q. (2012). Hydrogeochemistry of High-Temperature Geothermal Systems in China: A Review. *Appl. Geochem.* 27 (10), 1887–1898. doi:10.1016/j.apgeochem.2012.07.006

Hao, Y., Pang, Z., Tian, J., Wang, Y., Li, Z., Li, L., et al. (2020). Origin and Evolution of Hydrogen-Rich Gas Discharges from a Hot spring in the Eastern Coastal Area of China. *Chem. Geol.* 538, 119477. doi:10.1016/j.chemgeo.2020.119477

Hilton, D. R., Fischer, T. P., and Marty, B. (2002). Noble Gases and Volatile Recycling at Subduction Zones. *Rev. Mineralogy Geochem.* 47 (1), 319–370. doi:10.2138/rmg.2002.47.9

Hochstein, M. P., and Regenauer–Lieb, K. (1998). Heat Generation Associated with Collision of Two Plates: the Himalayan Geothermal belt. *J. Volcanol. Geoth. Res.* 83 (1–2), 75–92. doi:10.1016/S0377–0273(98)00018–3

Hoke, L., Lamb, S., Hilton, D. R., and Poreda, R. J. (2000). Southern Limit of Mantle–Derived Geothermal Helium Emissions in Tibet: Implications for Lithospheric Structure. *Earth Planet. Sci. Lett.* 180 (3–4), 297–308. doi:10.1016/S0012–821X(00)00174–6

Hu, S., He, L., and Wang, J. (2000). Heat Flow in the continental Area of China: a New Data Set. *Earth Planet. Sci. Lett.* 179 (2), 407–419. doi:10.1016/s0012-821x(00)00126-6

Javoy, M., Pineau, F., and Delorme, H. (1986). Carbon and Nitrogen Isotopes in the Mantle. *Chem. Geol.* 57 (1–2), 41–62. doi:10.1016/0009-2541(86)90093-8

Jiang, G., Hu, S., Shi, Y., Zhang, C., Wang, Z., and Hu, D. (2019). Terrestrial Heat Flow of continental China: Updated Dataset and Tectonic Implications. *Tectonophysics* 753, 36–48. doi:10.1016/j.tecto.2019.01.006

Jolie, E., Moeck, I., and Faulds, J. E. (2015). Quantitative Structural-Geological Exploration of Fault-Controlled Geothermal Systems-A Case Study from the Basin-and-Range Province, Nevada (USA). *Geothermics* 54, 54–67. doi:10.1016/j.geothermics.2014.10.003

Li, Z. X., Li, X. H., Wartho, J. A., Clark, C., Li, W. X., Zhang, C. L., et al. (2010). Magmatic and Metamorphic Events during the Early Paleozoic Wuyi-Yunkai Orogeny, southeastern South China: New Age Constraints and Pressure-Temperature Conditions. *Geol. Soc. Am. Bull.* 122 (5–6), 772–793. doi:10.1130/B30021.1

Li, X.-H., Li, Z.-X., He, B., Li, W.-X., Li, Q.-L., Gao, Y., et al. (2012). The Early Permian Active continental Margin and Crustal Growth of the Cathaysia Block: *In Situ* U-Pb, Lu-Hf and O Isotope Analyses of Detrital Zircons. *Chem. Geol.* 328, 195–207. doi:10.1016/j.chemgeo.2011.10.027

Li, J., Pang, Z., Yang, G.-M., Tian, J., Tong, A. L., Zhang, X.-Y., et al. (2017). Million-year-old Groundwater Revealed by Krypton-81 Dating in Guanzhong Basin, China. *Sci. Bull.* 62 (17), 1181–1184. doi:10.1016/j.scib.2017.08.009

Li, S., Suo, Y., Li, X., Zhou, J., Santosh, M., Wang, P., et al. (2019). Mesozoic Tectono-Magmatic Response in the East Asian Ocean-Continent Connection Zone to Subduction of the Paleo-Pacific Plate. *Earth-Sci. Rev.* 192, 91–137. doi:10.1016/j.earscirev.2019.03.003

Li, X.-h. (2000). Cretaceous Magmatism and Lithospheric Extension in Southeast China. *J. Asian Earth Sci.* 18 (3), 293–305. doi:10.1016/s1367-9120(99)00060-7

Liao, Z., and Zhao, P. (1999). *Yunnan–Tibet Geothermal belt–geothermal Resources and Case Histories*. Beijing: Science. (in Chinese with English abstract).

Lowenstern, J. B., Bergfeld, D., Evans, W. C., and Hunt, A. G. (2015). Origins of Geothermal Gases at Yellowstone. *J. Volcanol. Geotherm. Res.* 302, 87–101. doi:10.1016/j.jvolgeores.2015.06.010

Lupton, J. E. (1983). TERRESTRIAL INERT GASES: Isotope Tracer Studies and Clues to Primordial Components in the Mantle. *Annu. Rev. Earth Planet. Sci.* 11, 371–414. doi:10.1146/annurev.ea.11.050183.002103

Mao, X., Wang, Y., Zhan, H., and Feng, L. (2015). Geochemical and Isotopic Characteristics of Geothermal Springs Hosted by Deep-Seated Faults in Dongguan Basin, Southern China. *J. Geochem. Explor.* 158, 112–121. doi:10.1016/j.gexplo.2015.07.008

Mao, X., Zhu, D., Ndikubwimana, I., He, Y., and Shi, Z. (2021). The Mechanism of High-Salinity thermal Groundwater in Xinzhou Geothermal Field, South China: Insight from Water Chemistry and Stable Isotopes. *J. Hydrol.* 593, 125889. doi:10.1016/j.jhydrol.2020.125889

Newell, D. L., Jessup, M. J., Cottle, J. M., Hilton, D. R., Sharp, Z. D., and Fischer, T. P. (2008). Aqueous and Isotope Geochemistry of Mineral Springs along the Southern Margin of the Tibetan Plateau: Implications for Fluid Sources and Regional Degassing of CO_2. *Geochem. Geophys. Geosyst.* 9 (8). doi:10.1029/2008GC002021

O'nions, R. K., and Oxburgh, E. R. (1988). Helium, Volatile Fluxes and the Development of continental Crust. *Earth Planet. Sci. Lett.* 90 (3), 331–347. doi:10.1016/0012–821X(88)90134–3

O'nions, R. K., and Oxburgh, E. R. (1983). Heat and Helium in the Earth. *Nature* 306 (5942), 429–431. doi:10.1038/306429a0

Pang, J., Pang, Z., Lv, M., Tian, J., and Kong, Y. (2018). Geochemical and Isotopic Characteristics of Fluids in the Niutuozhen Geothermal Field, North China. *Environ. Earth Sci.* 77 (1), 12. doi:10.1007/s12665-017-7171-y

Pei, R., and Hong, D. (1995). The Granites of South China and Their Metallogeny. *Episodes* 18, 77–82. doi:10.18814/epiiugs/1995/v18i1.2/017

Polyak, B. G., Tolstikhin, I. N., and Yakutseni, V. P. (1979). The Isotopic Composition of Helium and Heat–Flow–Geochemical and Geophysical Aspects of Tectogenesis. *Geotectonics* 13 (5), 339–351.

Polyak, B. G., Tolstikhin, I. N., Kamensky, I. L., Yakovlev, L. E., Cheshko, A. L., and Marty, B. (2000). Helium Isotopes, Tectonics and Heat Flow in the Northern Caucasus. *Geochim. Cosmochim. Acta* 64 (11), 1925–1944. doi:10.1016/s0016-7037(00)00342-2

Qiu, X., Wang, Y., Wang, Z., Regenauer-Lieb, K., Zhang, K., and Liu, J. (2018). Determining the Origin, Circulation Path and Residence Time of Geothermal Groundwater Using Multiple Isotopic Techniques in the Heyuan Fault Zone of Southern China. *J. Hydrol.* 567, 339–350. doi:10.1016/j.jhydrol.2018.10.010

Sano, Y., and Marty, B. (1995). Origin of Carbon from Fumarolic Gas in Island Arc. *Chem. Geol.* 119 (1), 265–274. doi:10.1016/0009-2541(94)00097-r

Sano, Y., and Wakita, H. (1985). Geographical Distribution of3He/4He Ratios in Japan: Implications for Arc Tectonics and Incipient Magmatism. *J. Geophys. Res.* 90 (B10), 8729–8741. doi:10.1029/JB090iB10p08729

Sano, Y., Kinoshita, N., Kagoshima, T., Takahata, N., Sakata, S., Toki, T., et al. (2017). Origin of Methane-Rich Natural Gas at the West Pacific Convergent Plate Boundary. *Sci. Rep.* 7 (1), 15646. doi:10.1038/s41598-017-15959-5

Santilano, A., Manzella, A., Gianelli, G., Donato, A., Gola, G., Nardini, I., et al. (2015). Convective, Intrusive Geothermal Plays: what about Tectonics. *Geoth. Energ. Sci.* 3 (1), 51–59. doi:10.5194/gtes–3–51–201510.5194/gtes-3-51-2015

Shu, L. S., Zhou, X. M., Deng, P., Wang, B., Jiang, S. Y., Yu, J. H., et al. (2009). Mesozoic Tectonic Evolution of the Southeast China Block: New Insights from

basin Analysis. *J. Asian Earth Sci.* 34 (3), 376–391. doi:10.1016/j.jseaes.2008.06.004

Smith, N. J. P., Shepherd, T. J., Styles, M. T., and Williams, G. M. (2005). Hydrogen Exploration: A Review of Global Hydrogen Accumulations and Implications for Prospective Areas in NW Europe. *Pet. Geology. Conf. Ser.* 6 (2), 349–358. doi:10.1144/0060349

Tang, X., Zhang, J., Pang, Z., Hu, S., Tian, J., and Bao, S. (2017). The Eastern Tibetan Plateau Geothermal belt, Western China: Geology, Geophysics, Genesis, and Hydrothermal System. *Tectonophysics* 717, 433–448. doi:10.1016/j.tecto.2017.08.035

Tannock, L., Herwegh, M., Berger, A., Liu, J., and Regenauer-Lieb, K. (2020). The Effects of a Tectonic Stress Regime Change on Crustal-Scale Fluid Flow at the Heyuan Geothermal Fault System, South China. *Tectonophysics* 781, 228399. doi:10.1016/j.tecto.2020.228399

Tian, J., Pang, Z., Guo, Q., Wang, Y., Li, J., Huang, T., et al. (2018). Geochemistry of Geothermal Fluids with Implications on the Sources of Water and Heat Recharge to the Rekeng High-Temperature Geothermal System in the Eastern Himalayan Syntax. *Geothermics* 74, 92–105. doi:10.1016/j.geothermics.2018.02.006

Tian, J., Pang, Z., Liao, D., and Zhou, X. (2021). Fluid Geochemistry and its Implications on the Role of Deep Faults in the Genesis of High Temperature Systems in the Eastern Edge of the Qinghai Tibet Plateau. *Appl. Geochem.* 131, 105036. doi:10.1016/j.apgeochem.2021.105036

Tong, W., and Tobisch, O. (1996). Deformation of Granitoid Plutons in the Dongshan Area, Southeast China: Constraints on the Physical Conditions and Timing of Movement along the Changle–Nanao Shear Zone. *Tectonophysics* 267 (1–4), 303–316. doi:10.1016/s0040-1951(96)00107-2

Umeda, K., Kanazawa, S., Kakuta, C., Asamori, K., and Oikawa, T. (2006). Variations in the 3 He/4 He Ratios of hot springs on Shikoku Island, Southwest Japan. *Geochem. Geophys. Geosyst.* 7 (4). doi:10.1029/2005GC001210

Wang, J., and Li, Z. (2003). History of Neoproterozoic Rift Basins in South China: Implications for Rodinia Break–Up. *Precambrian Res.* 122 (1–4), 141–158. doi:10.1016/s0301-9268(02)00209-7

Wang, Y. (1999). A Study on Mantle Heat Flow of continental Area of China by Helium Isotope Ratio of the Underground Fluid. *Acta Geoscientia Sinica* 20, 48–50. (in Chinese with English abstract).

Wilson, R. M., Macelloni, L., Simonetti, A., Lapham, L., Lutken, C., Sleeper, K., et al. (2014). Subsurface Methane Sources and Migration Pathways within a Gas Hydrate mound System, Gulf of Mexico. *Geochem. Geophys. Geosyst.* 15 (1), 89–107. doi:10.1002/2013gc004888

Wu, L., Mei, L., Paton, D. A., Guo, P., Liu, Y., Luo, J., et al. (2018). Deciphering the Origin of the Cenozoic Intracontinental Rifting and Volcanism in Eastern China Using Integrated Evidence from the Jianghan Basin. *Gondwana Res.* 64, 67–83. doi:10.1016/j.gr.2018.07.004

Yan, X., Gan, H., and Yue, G. (2019). Hydrogeochemical Characteristics and Genesis of Typical Geothermal fields from Huangshadong to Conghua in Guangdong. *Geol. Rev.* 65 (3), 743–754. CNKI:SUN:DZLP.0.2019-03-020 (in Chinese with English abstract).

Yin, A. (2010). Cenozoic Tectonic Evolution of Asia: A Preliminary Synthesis. *Tectonophysics* 488 (1–4), 293–325. doi:10.1016/j.tecto.2009.06.002

Zhang, M., Guo, Z., Sano, Y., Zhang, L., Sun, Y., Cheng, Z., et al. (2016). Magma-derived CO_2 Emissions in the Tengchong Volcanic Field, SE Tibet: Implications for Deep Carbon Cycle at Intra-continent Subduction Zone. *J. Asian Earth Sci.* 127, 76–90. doi:10.1016/j.jseaes.2016.06.009

Zhang, M., Guo, Z., Xu, S., Barry, P. H., Sano, Y., Zhang, L., et al. (2021). Linking Deeply–Sourced Volatile Emissions to Plateau Growth Dynamics in southeastern Tibetan Plateau. *Nat. Commun.* 12 (1), 1–10. doi:10.1038/s41467-021-24415-y

Zhao, G., Wilde, S. A., Cawood, P. A., and Lu, L. (1998a). Thermal Evolution of Archean Basement Rocks from the Eastern Part of the North China Craton and its Bearing on Tectonic Setting. *Int. Geology. Rev.* 40 (8), 706–721. doi:10.1080/00206819809465233

Zhao, P., Dor, J., Liang, T., Jin, J., and Zhang, H. (1998b). Characteristics of Gas Geochemistry in Yangbajing Geothermal Field, Tibet. *Chin. Sci. Bull.* 43 (21), 1770–1777. doi:10.1007/BF02883369

Zhao, P., Xie, E., Duo, J., Jin, J., Hu, X., Du, S., et al. (2002). Geochemical Characteristics of Geothermal Gases and Their Geological Implications in Tibet. *Acta Petrol. Sin.* 18 (4), 539–550. doi:10.1002/poc.1772

Zhao, C., Ran, H., and Chen, K. (2011). Presen–Day Temperatures of Magma chambers in the Crust beneath Tengchong Volcanic Field: Estimation from Carbon Isotopic Fractionation between CO_2 and CH_4 of Free Gases Escaped from thermal Springs. *Acta Petrol. Sin.* 27 (10), 2883–2897. (in Chinese with English abstract). CNKI:SUN:YSXB.0.2011–10–009.

Zhou, X., and Li, W. (2000). Origin of Late Mesozoic Igneous Rocks in Southeastern China: Implications for Lithosphere Subduction and Underplating of Mafic Magmas. *Tectonophysics* 326 (3–4), 269–287. doi:10.1016/s0040-1951(00)00120-7

Zhou, X., Sun, T., Shen, W., Shu, L., and Niu, Y. (2006). Petrogenesis of Mesozoic Granitoids and Volcanic Rocks in South China: A Response to Tectonic Evolution. *Episodes* 29 (1), 26–33. doi:10.18814/epiiugs/2006/v29i1/004

Zhou, X., Liu, L., Chen, Z., Cui, Y., and Du, J. (2017). Gas Geochemistry of the Hot spring in the Litang Fault Zone, Southeast Tibetan Plateau. *Appl. Geochem.* 79, 17–26. doi:10.1016/j.apgeochem.2017.01.022

Conflict of Interest: The authors declare that the research was conducted in the absence of any commercial or financial relationships that could be construed as a potential conflict of interest.

Publisher's Note: All claims expressed in this article are solely those of the authors and do not necessarily represent those of their affiliated organizations, or those of the publisher, the editors, and the reviewers. Any product that may be evaluated in this article, or claim that may be made by its manufacturer, is not guaranteed or endorsed by the publisher.